High-speed image edge detector based on thin-film lithium niobate

Hanke Feng
Department of Electrical Engineering & State Key Laboratory of Terahertz and Millimeter Waves, City University of Hong Kong, Kowloon, Hong Kong, China
hankefeng2-c@my.cityu.edu.hk

Tong Ge
Department of Electrical Engineering, City University of Hong Kong, Kowloon, Hong Kong, China
tongge3-c@my.cityu.edu.hk

Xiaoqing Guo
Department of Electrical Engineering, City University of Hong Kong, Kowloon, Hong Kong, China
xiaoqingguo1128@gmail.com

Yixuan Yuan
Department of Electronic Engineering, Chinese University of Hong Kong, Shatin, Hong Kong, China
yxyuan@ee.cuhk.edu.hk

Cheng Wang
Department of Electrical Engineering & State Key Laboratory of Terahertz and Millimeter Waves, City University of Hong Kong, Kowloon, Hong Kong, China
cwang257@cityu.edu.hk

***Abstract*—We report a high-speed image edge detector based on an integrated lithium niobate photonic chip with processing sampling rates up to 92 GSa/s. We further use the devices to realize photonics-assisted segmentation of medical images.**

***Keywords*—thin-film lithium niobate, microwave photonics, image edge detection, medical diagnosis**

I. INTRODUCTION

With the rapid expansion of wireless networks and Internet of Things (IoTs), the electronic bandwidth and performance of underlying radio frequency (RF) systems are facing severe challenges [1]. Meanwhile, the ever-growing artificial intelligence (AI) technologies also demand ultrahigh-speed, low-power, and low-latency processing and computation of analog signals much beyond those offered by traditional electronic integrated circuits. Microwave photonics (MWP) can provide efficient solutions to address these challenges through the usage of optical devices to perform microwave signal generation, transmission and manipulation tasks [2]. Recently, the surge of photonics integration technologies has led to a dramatic reduction in size, weight, and power of the MWP system with enhanced robustness and functionalities [3]. The recently emerged thin-film lithium niobate (LN) platform is a promising candidate for integrated MWP signal processing owing to its unique electro-optic properties, low optical loss and excellent scalability [4-6].

Here, we demonstrate a high-speed image edge-feature detector based on LN platform, realizing high-speed analog computation of electronic signals up to 92 GSa/s. We further plug the photonics-assisted image-edge detector into a neural network-based image segmentation model, to showcase the effective identification of melanoma lesion outlines in medical diagnostic images.

II. HIGH-SPEED IMAGE EDGE DETECTOR

Figure 1 demonstrates the schematic diagram of high-speed image edge-feature detector, including a high-speed phase modulator (PM) and an MZI-based signal processor, together on thin-film LN platform. The RGB information of two-dimension (2D) images are grayed and serialized into a time-domain data stream, and up-converted to optical domain by modulators. The MZI-based signal processing unit performs a real-time differentiation process of the data stream [7, 8]. Finally, we de-multiplex the captured time-series data back into matrix format to form the reconstructed image with clear edge information.

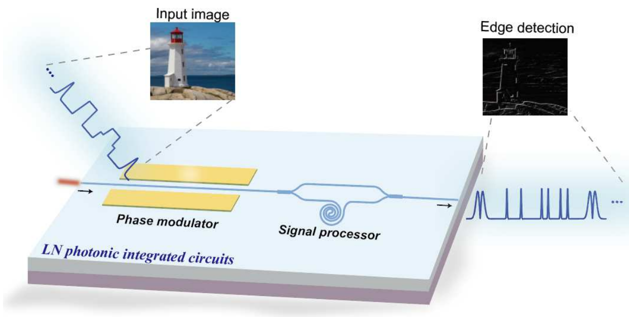

Fig. 1. Schematic diagram of high-speed image edge detector based on thin-film LN platfrom.

The basic working principle of on-chip signal processing section is shown in Fig. 2a: the input RF signal $x(t)$ is first loaded on a continuous-wave (CW) optical signal by the PM, leading to an instantaneous optical phase of $\omega_0 + \beta x(t)$, where ω_0 is the carrier frequency of the signal and β is the modulation index. This induces an instantaneous frequency chirp of $\omega_0 + \beta \frac{dx(t)}{dt}$ that exactly follows the differentiation of the input signal $\frac{dx(t)}{dt}$. The chirped frequency information is then mapped into optical field using a signal processing unit, i.e. an unbalanced MZI in this case. When biasing the MZI at the null point, where the output optical field is linearly proportional to the optical frequency, the output RF signals are exactly the differentiation form of input signals [7]. Fig. 2b shows the experimental setup, inset is the microscope image of the device. The measured transfer function of the unbalanced MZI is shown in Fig. 2c, consistent with the ideal linear response within a processing bandwidth of 40 GHz, limited by FSR.

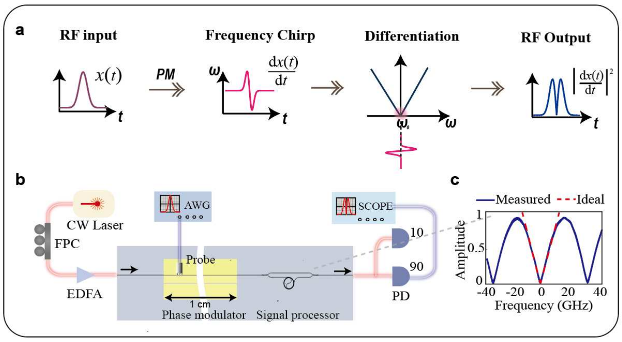

Fig. 2. High-speed on-chip image edge dection system. a. Working principle of the frequency-chirp-based temporal differentiation process. b. Experimental setup for the measurement of image edge detector. Inset shows a microscope image of the device. c. Measured and ideal transfer functions of the MZI-based signal processor.

We firstly test the fundamental performance by injecting a sequence of RF signals including Gaussian pulses (FWHM ~ 90ps, 120ps), square pulses (FWHM ~ 300ps, 500ps) and stepped pulses [Fig. 3a (red)] into the phase modulator. The blue trace shows the corresponding measured output results, where the pulse height is determined by the temporal rising/falling slope of input signals. Here the output signals are positive for both rising and falling edges since the differentiation result in the form of optical field is measured by a direct intensity detection at the PD showing $\left|\frac{dx(t)}{dt}\right|^2$. The bottom panels of Fig. 3a show blow-up views of input and output waveforms together with the ideal ones, showing an average accuracy of 96.47%. The slight mismatch is mainly originated from the limited analog bandwidth of our AWG.

Next, we showcase the power of our edge-feature detector by feeding the system with a 250×250-pixel 'CityU' logo in Fig. 3b, serialized as a 92 GSa/s data stream. The edge detection functions are performed "on-the-fly" within a short time ($250\times250\times\frac{1}{92\ \mathrm{GSa/s}} = 679$ ns) and captured by a real-time oscilloscope. We de-multiplex the captured time-series data back into matrix format, showing clearly resolved edge features. The processing speed could be readily increased to at least 200 GSa/s considering the large analog bandwidth of our EO modulator deep into the millimeter-wave band [9, 10], currently limited by the sampling rate of our AWG.

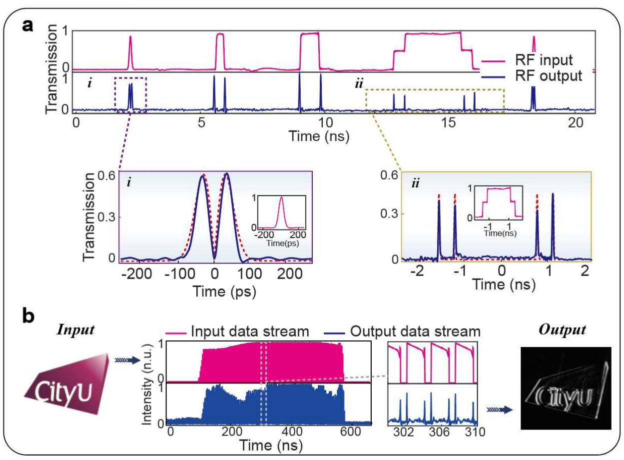

Fig. 3. Experimental analysis of our image edge detector. a. Measured fundemental response (blue) for a sequence of input RF signals (red). Blow-up panels show the measured (blue solid) and ideal (red dashed) results for a Gaussian pulse (*i*) and a stepped pulse (*ii*) (see insets). b. image edge detection of a 250×250-pixel 'CityU' logo.

III. High-speed Photonic-assisted Image Segmentation System

When processing complex and often low-contrast medical images, the fuzzy boundaries between abnormal and normal regions could lead to compromised accuracies of lesion predictions. This situation could be substantially improved by feeding the deep convolution neutral network (DCNN) with edge-detected information instead of original images, which can be integrated into an arbitrary encoder-decoder architecture in an end-to-end way for medical image segmentation process [11]. Based on the above scheme, we plug our high-speed photonic-assisted image edge detector into a DCNN-based image segmentation model for outlining the boundaries of medical diagnostic images with superior processing speed and accuracy, which can provide quantitative analysis to help clinicians conduct prompt and accurate disease diagnosis and treatment.

Figure 4a-b illustrates the flow diagram and working principle of the proposed edge-enhanced DCNN segmentation model that intakes raw RGB images and outputs segmentation results [12, 13]. To optimize the segmentation model, we first train the model with concatenated dermoscope images and the corresponding melanoma edge information derived from simulated differentiation, emphasizing the representations around melanoma lesion boundaries [14]. Based on the optimized model, the test dermoscope images are concatenated with experimentally extracted lesion edge information to generate the melanoma region prediction. Figure 4c shows the original melanoma lesion images captured from dermoscope, simulated and experimentally measured edge features, as well as the lesion regions segmented by our model, respectively. The tested average segmentation accuracy of our edge-facilitated model is 95.44 %, proving the effectiveness of the proposed photonic-assisted segmentation model.

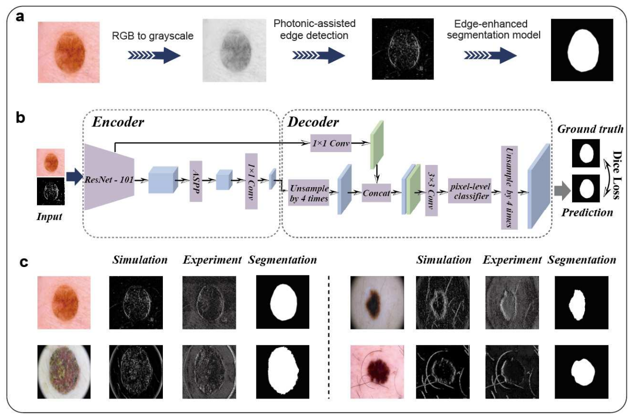

Fig. 4. High-speed photonic-assisted medical image segmentation. a. Flow diagram of photonic-assisted image segmentation model. The edge features of melanoma legion images are extracted by our LN-based image-edge detector and passed through a DCNN-based segmentation model to obtain the lesion segmentation results. b. Fundamental principle of the image segmentation model. c. Examples of melanoma lesion segmentation results showing original dermoscope images, simulated and experimentally extracted edge features, as well as the lesion regions segmented by our model, respectively.

Furthermore, we make a detailed performance comparison between traditional electronics-based algorithms (including convolution-based and simple differentiation-based algorithms) and our photonic-assisted segmentation model in Table 1. The performance metrics include raw lesion edge detection accuracy (before DCNN), final segmentation accuracy (after DCNN), and computation time. The accuracies of lesion edge detection and segmentation are measured by dice coefficient [12]. Our photonic edge detector shows a better raw edge detection accuracy (23.5%) than those of both convolution-based (18.1%) and differentiation-based (12.8%) algorithms, mainly because it picks up less false-positive details inside the lesion region. The final image segmentation accuracies are above 95% for all three methods but with drastically different processing time. For edge feature extraction of a 250×250-pixel image, our device is nearly three orders of magnitude faster than performing a traditional convolution algorithm on a generic personal computer. Therefore, our demonstrated high-speed photonics-assisted image segmentation model could pave the path for high-complexity, high-throughput and real-time medical diagnosis tasks.

TABLE I. PERFORMANCE COMPARISON WITH TRADITIONAL ELECTRONICS-BASED ALGORITHMS

	Differentiation algorithm	**Convolution algorithm**	**This work**
Raw lesion edge detection *†	12.831%	18.149%	23.509%
Segmentation accuracy*	95.602%	95.888%	95.437%
Computation time	0.12 ms	0.38 ms	679 ns

* Detection and segmentation accuracies are measured by dice coefficient.
† Raw detection accuracy right after edge detection algorithms, before entering DCNN.

IV. CONCLUSION

In summary, we have demonstrated a high-speed and high-fidelity image edge detector based on thin-film LN platform, with processing sampling rates up to 92 GSa/s. We further combined the edge detection system with DCNN algorithm to realize photonics-assisted image segmentation model for medical diagnosis, providing three orders of magnitude faster processing speed than traditional algorithm.

ACKNOWLEDGMENT

We thank the funding of National Natural Science Foundation of China (61922092); Research Grants Council, University Grants Committee (CityU 11204820, CityU 21208219, N_CityU113/20); Croucher Foundation (9509005); City University of Hong Kong (9610402, 9610455).

REFERENCES

[1] V. Ilderem, "The technology underpinning 5G," Nat. Electron., vol. 3, no. 1, pp. 5-6, 2020.

[2] J. Capmany and D. Novak, "Microwave photonics combines two worlds," Nat. Photon., vol. 1, no. 6, p. 319, 2007.

[3] D. Marpaung, J. Yao, and J. Capmany, "Integrated microwave photonics," Nat. Photon., vol. 13, no. 2, pp. 80-90, 2019.

[4] A. Boes et al., "Lithium niobate photonics: Unlocking the electromagnetic spectrum," Science, vol. 379, no. 6627, p. eabj4396, 2023.

[5] D. Zhu et al., "Integrated photonics on thin-film lithium niobate," Advances in Optics and Photonics, vol. 13, no. 2, pp. 242-352, 2021.

[6] H. Feng et al., "Ultra-high-linearity integrated lithium niobate electro-optic modulators," Photonics Res., vol. 10, no. 10, pp. 2366-2373, 2022.

[7] J. Dong, A. Zheng, D. Gao, L. Lei, D. Huang, and X. Zhang, "Compact, flexible and versatile photonic differentiator using silicon Mach-Zehnder interferometers," Opt. Express, vol. 21, no. 6, pp. 7014-7024, 2013.

[8] W. Liu et al., "A fully reconfigurable photonic integrated signal processor," Nat. Photon., vol. 10, no. 3, pp. 190-195, 2016.

[9] C. Wang et al., "Integrated lithium niobate electro-optic modulators operating at CMOS-compatible voltages," Nature, vol. 562, no. 7725, pp. 101-104, 2018.

[10] Y. Zhang et al., "Systematic investigation of millimeter-wave optic modulation performance in thin-film lithium niobate," Photonics Res., vol. 10, no. 10, pp. 2380-2387, 2022.

[11] M. Zhang, F. Yu, J. Zhao, L. Zhang, and Q. Li, "BEFD: Boundary enhancement and feature denoising for vessel segmentation," in Medical Image Computing and Computer Assisted Intervention–MICCAI 2020: 23rd International Conference, Lima, Peru, October 4–8, Proceedings, Part V 23: Springer, pp. 775-785, 2020.

[12] F. Milletari, N. Navab, and S.-A. Ahmadi, "V-net: Fully convolutional neural networks for volumetric medical image segmentation," in 2016 fourth international conference on 3D vision (3DV),: IEEE, pp. 565-571, 2016.

[13] K. He, X. Zhang, S. Ren, and J. Sun, "Deep residual learning for image recognition," in Proceedings of the IEEE conference on computer vision and pattern recognition, pp. 770-778, 2016.

[14] N. C. Codella et al., "Skin lesion analysis toward melanoma detection," in 2018 IEEE 15th international symposium on biomedical imaging , IEEE, pp. 168-172, 2018.